Trop J Nat Prod Res, June 2025; 9(6): 2922 - 2932 **ISSN 2616-0684 (Print)**
ISSN 2616-0692 (Electronic)

Tropical Journal of Natural Product Research

Available online at https://www.tjnpr.org

Original Research Article

In Silico Studies of *Stylissa Carteri*-Compounds against EGFR and RAF Proteins in Triple-Negative Breast Cancer

Naufal Ma'arif [1,2,3,4], Anissa Nofita Sari[4], Wirdatun Nafisah[5], Annisa Krama[2,6], Hanum Isfaeni[1], Rusdi Rusdi[1], Gusnia M. Gholam[2,7].

[1]*Biology Education Department, Faculty of Mathematics and Natural Science, Universitas Negeri Jakarta, East Jakarta 13320, Indonesia*
[2] *Bioinformatics Research Center, INBIO Indonesia, Malang, 65162, Indonesia*
[3]*Magister Biology Program, Faculty of Mathematics and Natural Science+6, Universitas Brawijaya, Malang, 65145, Indonesia*
[4]*Research Center of Vaccine and Drug, Research Organization for Health, National Research and Innovation Agency (BRIN), Bogor, 16911, Indonesia*
[5]*Biology Department, Faculty of Mathematics and Natural Science, Universitas Negeri Surabaya, Surabaya, 60231, Indonesia*
[6]*Tsukuba-Plant Innovation Research Center, Institute of Life and Environmental Sciences, University of Tsukuba, Ibaraki, 305-8572, Japan*
[7]*Departement of Biochemistry, Faculty of Mathematics and Natural Sciences, Bogor Agricultural University, 16680, Bogor, Indonesia*

ARTICLE INFO

Article history:
Received 07 January 2025
Revised 30 April 2025
Accepted 07 May 2025
Published online 01 July 2025

ABSTRACT

Triple-negative breast cancer (TNBC) represents a highly aggressive form of breast cancer, and the treatment options available are regarded as particularly challenging. The lack of specific molecular targets, including estrogen receptor (ER), progesterone receptor (PR), and human epidermal growth factor receptor 2 (HER2), accounts for this situation. This study investigates the molecular interactions between natural compounds derived from Stylissa carteri and Epidermal Growth Factor Receptor (EGFR) and RAF proteins, which are promising targets for therapeutic strategies in triple-negative breast cancer (TNBC), utilizing in silico techniques. Nine compounds derived from Stylissa carteri were obtained from the Knapsack and PubChem servers. These compounds' biological activities and interactions with EGFR and RAF proteins were analyzed. The findings indicated that the nine compounds exhibited various biological activities inhibiting TNBC. Docking and molecular dynamics analysis revealed that stevensine and dibutyl phthalate exhibited the highest binding affinity and the most stable interactions with the EGFR-RAF protein complex. Docking analysis revealed binding affinity values between −5.4 and −7.9 kcal/mol. The most robust binding interaction was noted for (Z)-hymenialdisine with RAF (−7.9 kcal/mol), whereas 1,2-benzenediol exhibited the weakest interaction (−5.7 kcal/mol). Dibutyl phthalate exhibited the highest binding affinity for EGFR, measured at −7.0 kcal/mol. The findings indicate that compounds derived from Stylissa carteri exhibit potential efficacy in targeting EGFR and RAF in triple-negative breast cancer (TNBC).

Keywords: Epidermal Growth Factor Receptors, docking analysis, molecular dynamics, *Stylissa carteri*, Rapidly Accelerated Fibrosarcoma, Triple Negative Breast Cancer.

Introduction

Triple-negative breast cancer (TNBC) is a specific subtype of breast cancer, comprising 15-20% of all classifications. This condition is marked by the lack of estrogen receptor (ER), progesterone receptor (PR), and human epidermal growth factor 2 (HER2), resulting in an elevated risk of metastasis, increased invasiveness, and a more rapid growth rate.[1,2] Certain studies have indicated an elevated recurrence risk in triple-negative breast cancer linked to resistance to standard adjuvant treatment. [3,4] Consequently, the identification of therapeutic molecules through the targeting of possible biomarkers is essential for the development of effective treatments with reduced recurrence risk.EGFR (Epidermal Growth Factor Receptor) is recognized as a proto-oncogene that promotes cellular proliferation and survival. It is the prototype of the EGFR family, which includes ErbB2/HER2/Neu, ErbB3/HER3, and ErbB4/HER4. Numerous studies indicate that EGFR is more commonly overexpressed in triple-negative breast cancer (TNBC) than in other breast cancer subtypes. [5–7] The stimulation of signaling additionally facilitates angiogenesis and confers resistance to trastuzumab.[8] Ryan et al. demonstrated that the concurrent inhibition of EGFR and RAF enhances outcomes in BRAF-mutant colorectal cancer by preventing the reactivation of mitogen-activated protein kinase (MAPK) signaling pathways in these tumors.[9] Information regarding the treatment of TNBC through the targeting of both EGFR and RAF proteins is currently limited. *Stylissa carteri*, a species within the Porifera phylum, is frequently identified in Indonesia and has been documented as a potential anti-cancer agent. [10–13] An *in vitro* study indicated that the ethyl acetate fraction of *Stylissa carteri* exhibited cytotoxic effects on TNBC cells. [14,15] Furthermore, a through investigation into the molecular interactions between natural compounds from *Stylissa carteri* and EGFR and RAF proteins in the context of TNBC utilising an *in silico* approach remains absent. This study aims to address the gap by examining the potential of compounds derived from *Stylissa carteri* as therapeutic candidates for TNBC, focussing on the simultaneous targeting of EGFR and RAF.

Corresponding author; Email: anissa.nofita.sari@brin.go.id
Tel: +6281913031993

Citation: Ma'arif N, Sari N. A, Nafisah W, Krama A, Isfaeni H, Rusdi Rusdi, Gholam M. G. *In Silico* Studies of *Stylissa Carteri*-Compounds Against Egfr And Raf Proteins In Triple-Negative Breast Cancer. Trop. J. Nat. Prod. Res., 2025 9(6): 2922 - 2932 https://doi.org/10.26538/tjnpr/v9i6.77

Official Journal of Natural Product Research Group, Faculty of Pharmacy, University of Benin, Benin City, Nigeria.

Materials and Methods

Compounds screening

Natural compounds from Stylissa carteri were identified through literature reviews, as documented in several articles. [16–20] Numerous articles indicate. Furthermore, screening was conducted utilizing the Knapsack server (http://www.knapsackfamily.com/) to verify the identified compounds. The physicochemical properties were assessed, and the Lipinski rule served as the criterion for screening. The Lipinski rule of five emphasizes molecular weight, hydrogen bond donors, hydrogen bond acceptors, LogP, and molar reactivity. [21,22] The toxicity level was assessed using ADME (http://lmmd.ecust.edu.cn/admetsar2/) to evaluate the potential harm of the compound to the body. ADME evaluates human oral bioavailability, yielding either negative or positive outcomes. [23]

Protein-ligand preparation

The natural products utilized in this study were active compounds extracted from the Porifera Stylissa carteri. The compounds were sourced from the Knapsack server (http://www.knapsackfamily.com/) as detailed in Table 1.[24] Selected proteins were obtained from the Protein Data Bank (PDB) (https://www.rcsb.org/).[25] The selected proteins were EGFR and RAF which play a crucial role in the MAPK pathway. [26]

The 3D structure of the Stylissa carteri compounds was generated utilizing Marvin Sketch and Discovery Studio. The tools were employed to reduce energy and convert compounds into PDB format. Document.

Biological activity prediction

The biological activity of ligands was predicted utilizing the PASS server (https://www.way2drug.com/passonline/). The Pass server is capable of identifying potential compounds based on the Probable to Active (Pa) value. Compounds exhibiting a value greater than 0.7 can be anticipated to possess biological activity.

Molecular docking analysis

Molecular docking was conducted utilizing Autodock Vina within the PyRx 09.05 software environment.[27] The docking process targeted several proteins, specifically EGFR (PDB Code: 1M17) and RAF (PDB Code: 3OG7), which are involved in the MAPK pathway as macromolecules. Ligands were derived from active compounds of Stylissa carteri. The EGFR macromolecule was subsequently docked with the ligand utilizing a grid setting centered at (X: 27.820; Y: -3.776; Z: 54.157) and dimensions measured in angstroms (X: 54.375; Y: 44.966; Z: 44.202).[28]

Docking for the RAF protein (PDB code) was performed using a grid center set at coordinates (X: -1.511; Y: 1.513; Z: 5.108) and dimensions in angstroms of (X: 52.407; Y: 33.721; Z: 33.200). The outcomes were subsequently visualized utilizing Biovia Discovery Studio 2021.

Molecular dynamics (MD) simulation

Molecular dynamics (MD) simulation was conducted using GROMOS96 43a1 force field and GROMACS 5.1.4 package. [29] The analysis involved EGFR and RAF to assess the interaction strength between the two proteins. The structures were subsequently solubilized utilizing the SPC water model within a triclinic box. The system was reduced to 5000 steps through the application of the steepest descent method. The subsequent stage involved configuring the MD Simulation for NVT, NPT, and production phases. The NVT series (constant particle number, volume, and temperature) was succeeded by the NPT series (constant particle number, pressure, and temperature) at 298 K and 1 atm for a duration of 20 ns.

The MD trajectories were further examined using the GROMACS software package. This program was utilized to assess the root-mean-square deviation (RMSD), root-mean-square fluctuation (RMSF) of the rotational radius, and the quantity of hydrogen bonds. The binding energy of RMSF and MD was investigated using gmxhbond, gmxrms, gmxgyrate, gmxsasa, and gmxrmsf.

C1. The RMSD is the average of the atomic distances required to check the equilibrium and structural stability of the protein in the presence of ligands. [30] The values are also used to evaluate changes in protein MD as well as conformational stability of protein-ligand complexes. RMSD value was calculated using Equation 1:

$$RMSD = \sqrt{\frac{1}{N}\sum_{i=1}^{N}(X_i^m - X_i^1)^2 + (Y_i^m - Y_i^1)^2 + (Z_i^m - Z_i^1)^2} \quad (1)$$

Where xm, ym; zm, and x1; y1; and z1 represent the initial coordinates and trajectory coordinates at frame t, respectively. N is the number of atoms. C2. RMSF (root-mean-square fluctuation) is a value used to determine the flexibility of a protein affected by compounds that act as local variations of binding. The variation of this flexibility is a parameter that determines the tethering in the bond between the test compound and the target protein. The RMSF graph often shows the residues in terms of significant changes during the MD simulation. A high value indicates that the protein has a flexible domain. The RMSF parameter can be measured using Equation 2:

$$RMSF = \sqrt{\frac{1}{T}\sum_{i=1}^{T}(X_i - \bar{X})^2} \quad (2)$$

Where T demonstrates trajectory frame numbers $\bar{X}$, while i is the time-averaged position. C3. H-Bond represents non-covalent bonds formed between hydrogen atoms and electronegative atoms. The interaction of Hydrogen with the main chain and amide nitrogen stabilizes the secondary structure. Hydrogen bonds are also related to the protein structure stiffness. By analyzing and measuring the molecular proportion using simulation, H-bonds can be predictably determined.

C4. The Rg (Radius of Gyration) value is an indicator measured in MD parameters in addition to RMSD, RMSF, H-Bond, and Binding Free Energy. Rg is one of the basic indicators that play an important role in measuring the total size of the molecular chain. It evaluates the compactness and flexibility of a protein in the biological environment, comparing the protein structure over time with the hydrodynamic radius that can be monitored experimentally. The measurement of Rg is shown in Equation 3:

$$Rg: \sqrt{\frac{1}{N}\sum_{i=1}^{N}|r(i) - r_{center}|^2} \quad (3)$$

C5. The last analysis used as an indicator of parameters in MD testing is Protein Solvent Accessible Surface Area (SASA). This indicator plays a role in protein folding and stability through the identification of protein surfaces using Van der Waals bonds.

Results and Discussion

A total of 11 compounds were derived from *Stylissa carteri* through the literature study, but only nine were found in the PubChem database, including 1,2-Benzenediol, Dibutyl phthalate, 9,12-Octadecadienoic acid, (Z)-3-Bromohymenialdisine, (Z)-Debromohymenialdisine, (Z)-Hymenialdisine, Debromohymenin, Hymenin, Oroidin, and Stevensine. These compounds were further tested, and the results are shown in Table 1. Subsequent examination was undertaken to explore the prospective efficacy of the compounds as agents against cancer. The natural compounds underwent screening in accordance with the Lipinski rule of five, resulting in a selection of qualified compounds that encompasses 1,2-benzenediol, dibutyl phthalate, (Z)-debromohymenialdisine, (Z)-hymenialdisine, debromohymenin, hymenin, oroidin, and stevensine. [34] Additionally, these compounds underwent evaluation to ascertain the degree of acute oral toxicity through the AdmetSar methodology. The findings indicated that dibutyl phthalate was categorized as toxicity class IV, exhibiting a probability of 0.64, while hymenin was placed in class II, demonstrating the highest acute oral toxicity level at 0.5121.[23,35.] These results indicate that the compounds used for molecular docking and dynamic analysis had a relatively low level of toxicity.

ISSN 2616-0684 (Print)
ISSN 2616-0692 (Electronic)

Table 1: The results of marine natural compounds screening from *Stylissa Carteri*

Nu	Compound Name	Chemical 3D Structure	CID	Lipinski Rule of Five	AdmetSar Results
1.	1,2-Benzenediol		289	mass: 169.000000 hydrogen bond donor: 5 hydrogen bond acceptors: 4 LOGP: 0.089900 Molar Refractivity: 43.785797	Oral toxicity : II (0.4487)
2.	Dibutyl phthalate	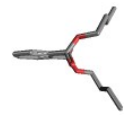	3026	mass: 278.000000 hydrogen bond donor: 0 hydrogen bond acceptors: 4 LOGP: 3.600399 Molar Refractivity: 76.822983	Oral toxicity : IV (0.6453)
3.	9,12-Octadecadienoic acid		3931	mass: 280.000000 hydrogen bond donor: 1 hydrogen bond acceptors: 2 LOGP: 5.884500 Molar Refractivity: 86.993774	Oral toxicity : IV (0.8289)
4	(Z)-Debromohymenialdisine	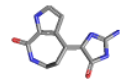	135451156	mass: 310.000000 hydrogen bond donor: 6 hydrogen bond acceptors: 3 LOGP: 0.767000 Molar Refractivity: 69.046692	Oral toxicity : III (0.5685)
5	(Z)-Hymenialdisine	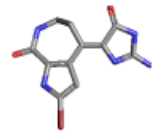	135413546	mass: 323.000000 hydrogen bond donor: 5 hydrogen bond acceptors: 6 LOGP: 0.066300 Molar Refractivity: 72.127998	Oral toxicity : III (0.5660)
6	Debromohymenin	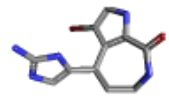	21775272	mass: 245.000000 hydrogen bond donor: 5 hydrogen bond acceptors: 6 LOGP: -0.696200 Molar Refractivity: 64.428001	Oral toxicity : III (0.5743)
7	Hymenin	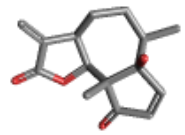	10499	mass: 262.000000 hydrogen bond donor: 1 hydrogen bond acceptors: 4 LOGP: 1.390400 Molar Refractivity: 68.111786	Oral toxicity : II (0.5136)
8	Oroidin	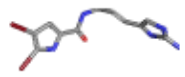	6312649	mass: 387.000000 hydrogen bond donor: 5 hydrogen bond acceptors: 4 LOGP: 2.288200 Molar Refractivity: 80.559990	Oral toxicity : III (0.5121)
9	Stevensine	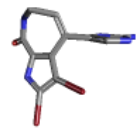	11003581	mass: 385.000000 hydrogen bond donor: 5 hydrogen bond acceptors: 4 LOGP: 2.020100 Molar Refractivity: 78.604996	Oral toxicity : III (0.5638)

Biological activity prediction

The potential activity (PA) and potential inactivity (PI) values were assessed utilizing the PASS server. Table 2 presents a comprehensive list of compounds that have been validated for their potential anti-cancer properties. The compound 1,2-benzenediol exhibited significant potential as a NADPH peroxidase (PA = 0.868) and as an inhibitor of

ISSN 2616-0684 (Print)
ISSN 2616-0692 (Electronic)

Table 2. Biological activities of *Stylissa carteri*-derived active compounds

No	Compound Name	Biological Activity	PA	PI
1	1,2-Benzenediol	NADPH peroxidase inhibitor	0.868	0.005
		G-protein-coupled receptor kinase inhibitor	0.769	0.016
		G-protein-coupled receptor kinase inhibitor	0.743	0.018
2	Dibutyl phthalate	NADH kinase inhibitor	0.603	0.013
3	9,12-Octadecadienoic acid	G-protein-coupled receptor kinase inhibitor	0.908	0.004
		NADH kinase inhibitor	0.758	0.005
4	(Z)-Debromohymenialdisine	MAP kinase 1 inhibitor	0.882	0.002
5	(Z)-Hymenialdisine	MAP kinase 1 inhibitor	0.977	0.000
		MAP3K5 inhibitor	0.785	0.001
6	Debromohymenin	Protein kinase (Mos, Mil/Raf, MEKK, RIPK, TESK, LIMK, IRAK, ILK, Activin/TGF-beta) inhibitor	0.695	0.003
7	Hymenin	Antineoplastic	0.959	0.004
8	Oroidin	MAP kinase 1 inhibitor	0.960	0.001
9	Stevensine	Protein kinase (Mos, Mil/Raf, MEKK, RIPK, TESK, LIMK, IRAK, ILK, Activin/TGF-beta) inhibitor	0.883	0.002
		MAP kinase 1 inhibitor	0.961	0.001
		Raf kinase inhibitor	0.664	0.003

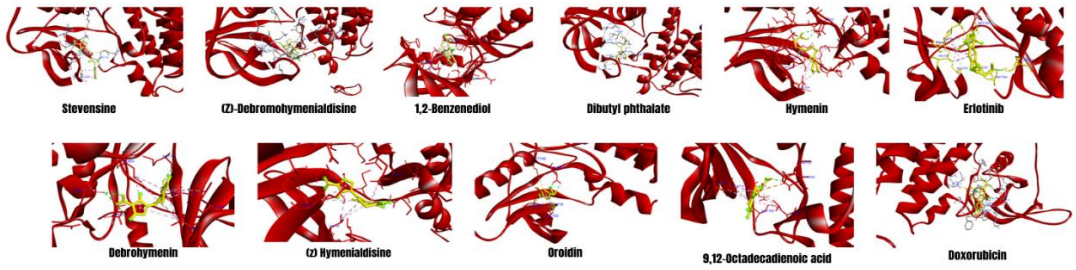

Figure 1. Docking analysis of *Stylissa carteri*-derived active compounds and native ligands with EGFR protein

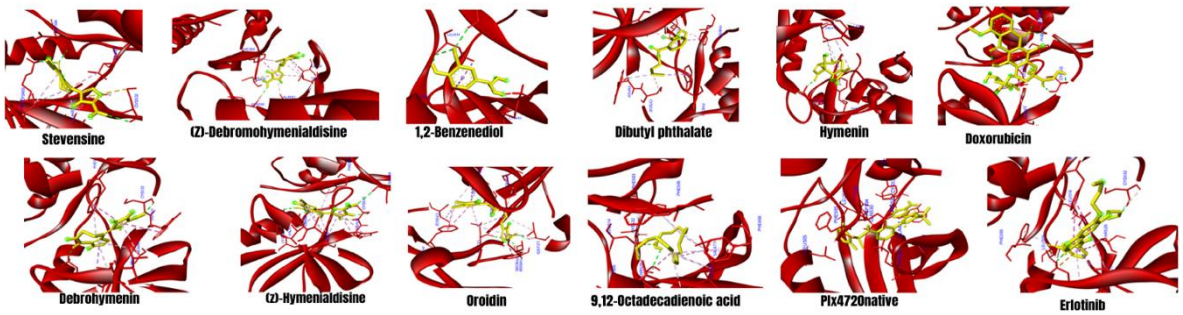

Figure 2. Docking analysis of *Stylissa carteri*-derived active compounds and native ligands with

Table 3. Docking analysis results in EGFR receptors

No	Compound Name	Binding Site	RMSD		Binding affinity
			ub	lb	
1	1,2-Benzenediol	Asp831, Cys773, Lys721, Leu820, Leu768, Leu694, Val702	1.173	1.073	-7
2	Dibutyl phthalate	Thr766, Met769 Leu 820 Val 702 THR830 Leu694 Lys721 Leu764 Met742	1.302	0.75	-6.6
3	9,12-Octadecadienoic acid	Met769, Gln767, Thr830, Asp831, Ala719, Leu820, Val 702	2.316	1.951	-7
4	(Z)-Debromohymenialdisine	Thr766, Lys721, Leu764, Met742, Leu694, Met769, Leu820, Val702	1.097	1.051	-6.5
5	(Z)-Hymenialdisine	Val702, Asp831, Lys721, Thr830, Unk, Leu820	3.017	2.299	-5.7
6	Debromohymenin	Met769, Thr766, Val702, Asp831, Arg817, Ala719, Leu694, Leu820	3.733	1.905	-5.6
7	Hymenin	Leu694, Ala719, Leu820, Val702, Lys721, Thr830	2.418	1.88	-5.4
8	Oroidin	Lys721, Met742, Leu764, Ala719, Asp831	2.037	1.081	-5.6
9	Stevensine	Asp831,	1.483	1.174	-6.5

No	Compound Name	Binding Site	RMSD		Binding affinity
			ub	lb	
		Cys773, Lys721, Leu820, Leu768, Leu694, Val702			
10	Doxorubicin (Kontrol)	Ala721, Ala719, Leu820, Leu694, Val702, Met769	1.509	1.139	-9.6
11	Erlotinib (Kontrol)	Val702, Cys773, Met769, Gun767, Leu764, Ala719, Thr766, Leu820, Lys721, Met742, Unk 0	1.718	1.424	-6.8

G-protein-coupled receptor kinase (GRK) (PA = 0.769). The compound dibutyl phthalate exhibited biological activity as a GRK inhibitor (PA = 0.743) and a NADPH kinase inhibitor (PA = 0.603). The compound 9,12-Octadecadienoic acid functioned as an inhibitor of GRK (PA = 0.908) and NADH kinase (PA = 0.758).

Additional analysis utilized an online Pass server (way2Drug) to evaluate the biological activities of compounds derived from Stylissa carteri, indicating their potential as anti-cancer agents. The results indicate that oroidin and debrohymenin may have direct interactions with RAF proteins, which are integral components of the MAPK pathway. Other compounds, including stevensine and dibutyl phthalate, exhibited potential interactions with NADH kinase inhibitors. These pathways are implicated in the regulation of the apoptosis mechanism in TNBC.[36,37] Therefore, docking analysis was performed on EGFR and RAF proteins, as the potential drug target in TNBC.

Molecular docking analysis

Molecular docking analysis was performed to assess the binding activities of compounds derived from Stylissa carteri to EGFR receptors, based on the evaluated biological activities (Table 3 and Fig. 1). A total of 10 compounds were ranked according to their binding affinity values, which are as follows: 1,2-benzenediol (-7), 9,12-octadecadienoic acid (-7), dibutyl phthalate (-6.9), (Z)-debromohymenialdisine (-6.6), stevensine (-6.5), (Z)-hymenialdisine (-6.5), debromohymenin (-5.7), oroidin (-5.6), hymenin (-5.6), and an additional compound (-5.4). The analysis indicated that hydrogen and hydrophobic bonds were involved in the interactions between compounds (ligands) and EGFR receptors. The compound 1,2-benzenediol exhibited interactions with several amino acids that are significant, including Asp831, Cys773, and Lys721, which participated in hydrogen bonding, while Leu820, Leu768, Leu694, and Val702 contributed to hydrophobic interactions. Dibutyl phthalate involves amino acids Thr766 and Met769 in hydrogen bonding, alongside Lys721, Leu764, Met742, Leu694, Leu820, and Val702 in hydrophobic interactions. The molecular docking of (Z)-debromohymenialdisine revealed the binding sites at Thr766, Lys721, Leu764, Met742, Leu694, Met769, Leu820, and Val702. The Stevensine compound contains amino acid residues such as Asp831, Cys773, Lys721, Leu820, Leu768, Leu694, and Val702.

Other compounds exhibit interactions involving hydrogen and hydrophobic bonds, including 9,12-octadecadienoic acid, which contains the residues Met769, Gln767, Thr830, Asp831, Ala719, Leu820, and Val702. Z-hymenialdisine comprises the amino acid residues Val702, Asp831, Lys721, Thr830, Unk, and Leu820. In contrast, debromohymenin includes Met769, Thr766, Val702, Asp831, Arg817, Ala719, Leu694, and Leu820. Oroidin contains amino acid residues including Lys721, Met742, Leu764, Ala719, Asp831, and Thr830. Hymenin contains amino acid residues including Leu694, Ala719, Leu820, Val702, Lys721, and Thr830.

The docking analysis results regarding the interactions between compounds derived from Stylissa carteri and RAF protein in the MAPK pathway are presented in Table 5 (Supplementary). The compound (Z)-hymenialdisine exhibited the highest binding affinity value of -7.9, while 1,2-benzendiol demonstrated the lowest at -5.7. The control compounds utilized were Doxorubicin, Erlotinib, and PLX4720 (native ligand).

The docking analysis of compounds derived from Stylissa carteri and RAF receptors was performed, focusing on binding affinity and RMSD values (Table 4 and Fig. 4). The most effective compounds identified were dibutyl phthalate, 9, 12 octadecadienoic acid, Z-hymenialdisine, oroidin, and stevensine, with binding affinities of -7, -7.1, -7.9, -7.3, and -7.5, respectively. Dibutyl phthalate exhibits hydrophobic interactions with Val471, Phe583, Cys532, Trp531, Leu505, and Phe595. The compound 9, 12-octadecadienoic acid exhibits hydrogen and hydrophobic interactions with the residues Phe468, Ile527, Phe595, Lys483, Val471, Phe583, Cys532, and Thr529. Simultaneously, Z-hymenialdisine exhibits hydrogen, hydrophobic, and unavoidable bump interactions with the amino acids Lys483, Ile463, Val471, Trp531, Gly534, Cys532, Phe583, and Ala481.Other compounds including oroidin and stevensine have hydrogen, hydrophobic, and unavoidable bump interactions. The amino acid residues in oroidin include Phe583, Lys483, Asp594, Leu514, Thr508, Leu505, Trp531, Ala481, Val471. Meanwhile, the amino acid residues in stevensine are Lys483, Asp594, Val471, Ala481, Leu514, and Cys532. Compounds 1,2-benzenediol, (Z)-debromohymenialdisine, debromohymenin, and hymenin also have hydrogen and hydrophobic interactions. In a docking analysis involving nine compounds with EGFR and RAF proteins, dibutyl phthalate and stevensine exhibited the highest binding affinity, characterized by hydrogen and hydrophobic interactions. Furthermore, these compounds exhibit analogous amino acid residues to those found in native ligands (see Table 3 and Table 4).

Interactions between Stevensine and EGFR involve residues Val702, Leu820, and Lys721, which are analogous to those of erlotinib, the native ligand. Doxorubicin exhibits interactions with the stevensine

Table 4. Docking analysis results in RAF receptors

No	Compound Name	Binding Site	RMSD		Binding affinity
			ub	lb	
1	1,2-Benzenediol	Lys483, Ile592, Leu514, Leu505	2.055	1.094	-5.7
2	Dibutyl phthalate	Phe468, Ile527, Phe595, Lys483, Val471, Phe583, Cys532, Thr529	1.886	1.479	-7
3	9,12-Octadecadienoic acid	Val471, Phe583, Cys532, Trp531, Leu505, Phe595	1.761	1.044	-7.1
4	(Z)-Debromohymenialdisine	Val471, Phe583, Cys532, Gln530, Ala481, Ile463	4.816	2.426	-6.7
5	(Z)-Hymenialdisine	Lys483, Ile463, Val471, Trp531, Gly534, Cys532, Phe583, Ala481	1.563	1.338	-7.9
6	Debromohymenin	Trp531, Phe583, Ile463, Cys532, Ala481, Val471, Lys483	2.770	2.309	-7.5
7	Hymenin	Cys532, Ile463, Phe583, Val471	2.824	1.790	-7.1
8	Oroidin	Phe583, Lys483, Asp594, Leu514, Thr508, Leu505, Trp531, Ala481, Val471	1.509	0.753	-7.3
9	Stevensine	Lys483, Asp594, Val471, Ala481, Leu514, Cys532	1.197	0.923	-7.5
10	Doxorubicin (Kontrol)	Phe583, Ile463, Ala481, Cys532, Leu514, Ser536,	2.013	1.439	-7.7

ISSN 2616-0684 (Print)
ISSN 2616-0692 (Electronic)

No	Compound Name	Binding Site	RMSD		Binding affinity
			ub	lb	
		Lys483			
11	PLX4720 (Kontrol)	THR529, ASP594, Val471, Phe583, Gln530, Ala481, Trp531, Cyss532, Lys483, Leu514, Gly593, Leu505, Phe595	1.41	0.027	-11.8
12	Erlotinib (Kontrol)	Cys532, Phe583, Val471, Lys483, Thr529, Leu514, Phe595, Ala481, Leu505, Unk0	1.410	1.104	-8.2

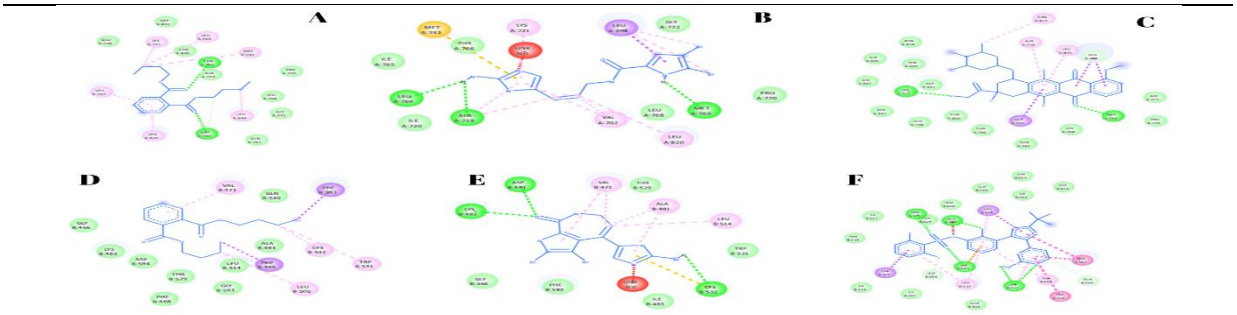

Figure 3. The visualization of molecular docking using discovery studio. EGFR interactions with (A) Dibutyl phthalate by hydrogen, hydrophobic, and van der walls interactions. (B) Stevensine by hydrogen, hydrophobic, unfavourable bump, and sulphur interactions. (C) Doxorubicin (control) by hydrogen, hydrophobic, and van der walls. RAF interactions with (D) Dibutyl phthalate by hydrogen, hydrophobic, and van der walls interactions. (E) Stevensine by hydrogen, hydrophobic, unfavorable bump, sulphur, and van der walls interactions. (F) Plx4720 (native ligand) by hydrogen, and hydrophobic.

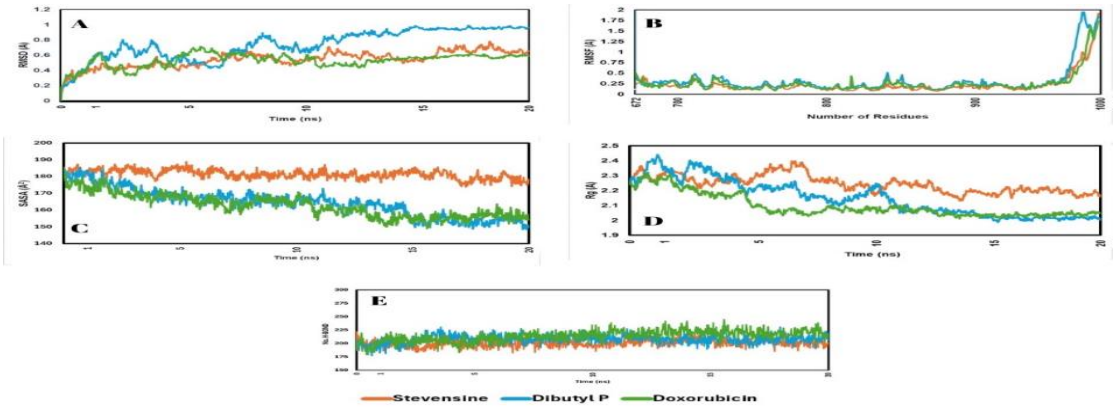

Figure 4. Molecular dynamics results on ligands - EGFR interactions. (A) RMSD values of the ligands. (B) RMSF spike values of each ligand. (C, D, E) SASA, Rg, and H-bond values, respectively, during the molecular dynamic simulation at 20 ns.

ligand comparable to those of erlotinib, specifically involving residues Leu820, Leu694, and Val702. Furthermore, stevensine and RAF engage with the amino acid residues Lys483, ASP594, Val471, Ala481, Leu514, and Cyss532. The interactions of these amino acid residues are also present in the native ligand PLX4720. The docking analysis showed that dibutyl phthalate and stevensine had the best interactions with EGFR and RAF protein (Table 3 and Fig 2; Table 4 and Fig 4). This was supported by the two-dimensional analysis in

Table 6 (supplementary), showing there is a consistent hydrogen bond in the interactions with EGFR at residue MET 769, and RAF at residues CYS 532, ASP 594, LYS 483, and VAL 471. Furthermore, MD analysis was

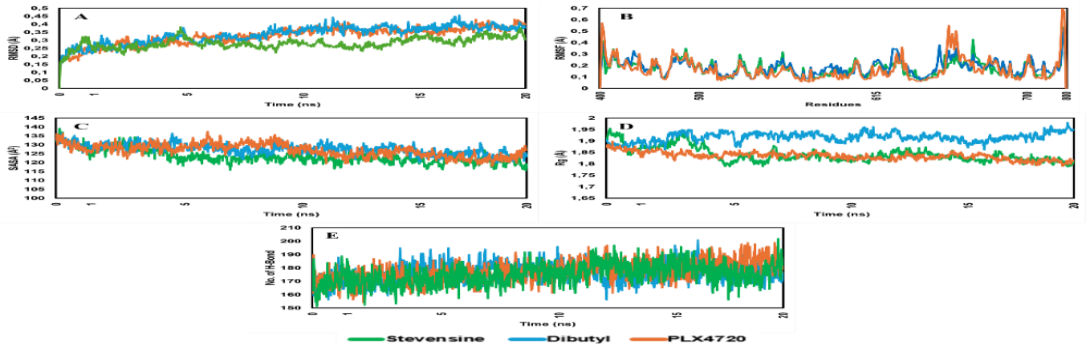

Figure 5. Molecular dynamics results on ligands – RAF interactions. (A) RMSD values of the ligands. (B) RMSF spike values of each ligand. (C, D, E) SASA, Rg, and H-bond values, respectively, during the molecular dynamic simulation at 20 ns.

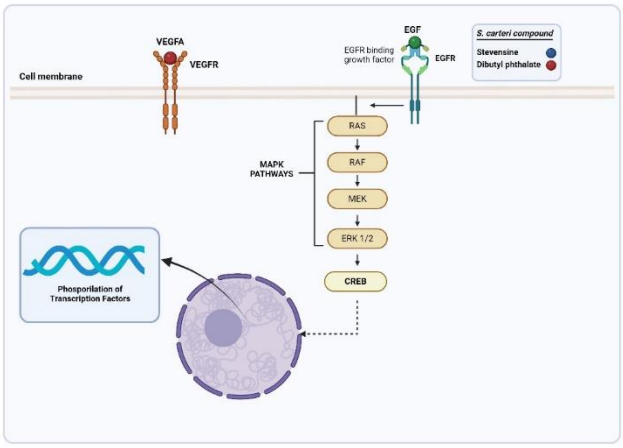

Figure 6. The EGFR pathway is associated with MAPK pathways by triggering the phosphorylation of transcription factors. The binding between *Stylissa carteri-derived* compounds EGFR (Epidermal Growth Factor Receptors) receptors with *Stylissa carteri* compounds (Stevensine & Dibutyl Phthalate). Inhibition of the MAPK pathway can trigger apoptosis in cells. [BioRender object]

conducted to determine the stability of the interactions between ligands and proteins. [38,39]

Molecular dynamics

Dibutyl phthalate and stevensine were evaluated for stability through molecular dynamics simulation using GROMACS 2019 over a duration of 20 ns in a physiological environment. The RMSD values over 20 ns presented in Fig. 5A indicate that the interactions between dibutyl phthalate and stevensine with EGFR were higher, measuring 0.54 nm and 0.73 nm, respectively, in comparison to doxorubicin (the native ligand), which had a value of 0.52 nm. The RMSF values (Fig. 5B) demonstrate that dibutyl phthalate exhibits the lowest fluctuation at 0.32 nm, in contrast to stevensine at 0.22 nm and doxorubicin at 0.25 nm in their interactions with EGFR. RMSF quantifies the flexibility of individual residues or atoms in molecular dynamics simulations, with lower values generally indicating decreased flexibility and enhanced stability of the protein-ligand complex. The lower RMSF value of dibutyl phthalate indicates a more effective stabilization of the EGFR binding region compared to stevensine and doxorubicin.

This interpretation aligns with molecular dynamics principles, indicating that smaller fluctuations suggest a more stable binding environment for the ligand within the protein structure. The observed differences among the ligands may indicate variations in binding modes, with dibutyl phthalate exhibiting increased rigidity around the active site residues. Previous studies have reported analogous correlations between low RMSF values and ligand stability. [31,32]

The SASA value indicates the measure of protein surface, which is important to determine the presence of Van der Waals[33]bonds on the protein surface. During the stimulation, stevensen showed higher SASA values (181 nm^2), compared to dibutyl phthalate (164 nm^2) and doxorubicin (162 nm^2) (Fig. 5C).

Rg indicates the density or compactness of the ligand-protein complex. Stevensine showed higher Rg value (2.24 nm), compared to dibutyl phthalate (2.15 nm) and doxorubicin (2.09 nm) (Fig. 5D). Furthermore, H-bond indicates the value of hydrogen bonds in the protein-ligand complex. The results showed doxorubicin has a higher H-bond value (200), followed by dibutyl phthalate (208) and stevensine (214) (Fig. 5E). The RMSD values presented in Fig. 6A indicate that dibutyl phthalate exhibited the highest value at 0.45 nm, followed by stevensine at 0.42 nm, and PLX4720 at 0.4 nm. Additionally, the RMSF values presented in Fig. 6B indicate that dibutyl phthalate and stevensine exhibit greater stability compared to PLX4720, with respective values of 0.172 nm, 0.186 nm, and 0.168 nm. Figure 6C shows the average SASA values calculated during the 20ns simulation for dibutyl phthalate which has the higher SASA value, compared to PLX4720 and stevensine, with respective values of 127 nm^2, 126 nm^2, and 123 nm^2. The Rg value of dibutyl phthalate was higher compared to stevensine and PLX4720 at 1.84nm, 1.91nm, and 1.83nm, respectively (Fig. 6D). The average H-bond values of PLX4720, dibutyl phthalate, and stevensine were 177, 176, and 174, respectively indicating that stevensine complex has the lowest number of H-bond compared to the other two complexes (Fig. 6E). The results of the MD analysis conducted with the 2019 version of Gromacs software on three EGFR and RAF protein-ligand complexes demonstrated favorable outcomes across five indicators: RMSD, RMSF, SASA, Rg, and H-bond. Figures 5 and 6 indicate that the RMSD results for the protein-ligand complexes exhibited fluctuations until reaching a duration of 10 ns. The RMSD value exhibited stability after a duration of 15 ns to 20 ns. The results indicated that the highest average value was 0.9 nm and below 3 Å, suggesting no significant conformational change in the complex structure of both EGFR and RAF proteins.[39–42]

The RMSF results presented in Fig. 6B indicate that the fluctuation in the values of EGFR and RAF protein complexes remained below 2.5 Å. The results were classified as low category, indicating that the EGFR and RAF protein-ligand complexes exhibited stable conformations. [43] The SASA value of stevensine for the EGFR protein complex exceeded that of dibutyl phthalate and doxorubicin. In the case of the RAF protein complex, the SASA value for the RAF-stevensine complex was lower than that of the other two complexes.

This indicates that the EGFR-stevensine complex value is less stable in comparison to RAF.

The RAF-stevensine complex exhibited the highest average Rg value among the EGFR protein complexes, followed by dibutyl phthalate and doxorubicin. This suggests that the tested ligands are more solid and compact in comparison to doxorubicin, which served as the control. The highest Rg value in the RAF protein complex was observed with dibutyl phthalate, followed by stevensine and PLX4720, indicating more robust and compact interactions compared to PLX4720 as a control. The H-bond value indicates whether the interaction between the complex and the ligand has a strong bond compared to covalent, hydrophobic, and Van der Waals bonds. [44] The MD results indicated that the most favorable hydrogen bonds in EGFR complexes were derived from doxorubicin, followed by dibutyl phthalate and stevensine. The RAF complex with PLX4720 exhibits a greater number of hydrogen bonds than the other two complexes, indicating stronger interactions in the control relative to the test ligands.

This study elucidates the molecular interactions between compounds derived from Stylissa carteri and EGFR and RAF proteins, identifying them as potential drug targets in TNBC cells, consistent with findings from Bashari et al. EGFR and RAF proteins, associated with MAPK pathways, are reported to engage in direct interactions (Fig. 7) that are crucial for inhibiting cell proliferation and inducing cell apoptosis via the autophagy mechanism.[37,45] As shown in Fig. 7, the mechanisms of cell proliferation inhibition through MAPK pathways comprise several proteins, such as RAS, RAF, MEK, and ERK. [46] Based on the in silico study, *Stylissa carteri*-derived compounds have good interactions with EGFR and RAF proteins suggesting great potential as drug targets in TNBC.

Conclusion

This study identifies the potential biological activities of natural compounds derived from Stylissa carteri in inhibiting essential proteins in TNBC. Stevensine and dibutyl phthalate exhibited the highest binding affinity values, averaging -5.7 for the EGFR complex and -7.6 for the RAF-ligand complex. The two compounds exhibited greater stability in their interactions with EGFR and RAF than the native ligands, doxorubicin and PLX4720. Additional research on in vitro studies is necessary to evaluate the anti-cancer properties of compounds derived from *Stylissa carteri* on various TNBC cell lines. A thorough examination of molecular signalling pathways, encompassing interactions with downstream proteins of EGFR and RAF, will enhance the understanding of the mechanisms behind the prevention of cancer cell proliferation. The development of appropriate pharmaceutical formulations, the analysis of resistance mechanisms, and the discovery of the biotransformation of active chemicals in biological systems are significant research domains.

Conflict of interest

The authors declare no conflict of interest.

Authors' Declaration

The authors hereby declare that the work presented in this article is original and that any liability for claims relating to the content of this article will be borne by them.

Acknowledgments

The authors would like to express their sincere gratitude to the Bioinformatics Research Center, INBIO Indonesia, for their invaluable support in utilizing resources and providing funding for the publication through the 2022 internship program.

References

1. Yao H, He G, Yan S, Chen C, Song L, Rosol TJ, Deng X. Triple-negative breast cancer: is there a treatment on the horizon? Oncotarget. 2016; 8(1):1913. Doi: 10.18632/oncotarget.12284
2. Zagami P, Carey LA. Triple negative breast cancer: Pitfalls and progress. NPJ breast cancer. 2022; 8(1):95. Doi: 10.1038/s41523-022-00468-0.
3. Bou Zerdan M, Ghorayeb T, Saliba F, Allam S, Bou Zerdan M, Yaghi M, Bilani N, Jaafar R, Nahleh Z. Triple negative breast cancer: updates on classification and treatment in 2021. Cancers. 2022; 14(5):1253. Doi: 10.3390/cancers14051253.
4. Obidiro O, Battogtokh G, Akala EO. Triple Negative Breast Cancer Treatment Options and Limitations: Future Outlook. Pharm. 2023; 15(7): 1796. Doi: 10.3390/pharmaceutics15071796.
5. Sukumar J, Gast K, Quiroga D, Lustberg M, Williams N. Triple-negative breast cancer: promising prognostic biomarkers currently in development. Expert Rev Anticancer Ther, 2021; 21(2):135-48. Doi: 10.1080/14737140.2021.1840984.
6. Bi J, Wu Z, Zhang X, Zeng T, Dai W, Qiu N, Xu M, Qiao Y, Ke L, Zhao J, Cao X. TMEM25 inhibits monomeric EGFR-mediated STAT3 activation in basal state to suppress triple-negative breast cancer progression. Nat. Commun, 2023; 14(1):2342. Doi: 10.1038/s41467-023-38115-2.
7. Masuda H, Zhang D, Bartholomeusz C, Doihara H, Hortobagyi GN, Ueno NT. Role of epidermal growth factor receptor in breast cancer. Breast Cancer Res. Treat, 2012; 136:331-45. Doi: 10.4103/2278-0513.155989.
8. Nami B, Maadi H, Wang Z. Mechanisms underlying the action and synergism of trastuzumab and pertuzumab in targeting HER2-positive breast cancer. Cancers, 2018;10(10):342. Doi: 10.3390/cancers10100342.
9. Pallela R, Ehrlich H. Marine sponges: Chemicobiological and biomedical applications. Marine Sponges: Chemicobiological and Biomedical Applications, 2016;1–381. Doi: 10.1007/978-81-322-2794-6.
10. Bhatnagar I. Marine sponges: Chemicobiological and biomedical applications. Pallela R, Ehrlich H, editors. New Delhi, India: Springer India; 2016. Doi: 10.1007/978-81-322-2794-6.
11. Bashari, M.H., Huda, F., Tartila, T.S., Shabrina, S., Putri, T., Qomarilla, N., Atmaja, H., Subhan, B., Sudji, I.R. and Meiyanto, E. Bioactive compounds in the ethanol extract of marine sponge *Stylissa carteri* demonstrates potential anti-cancer activity in breast cancer cells. Asian Pac. J. Cancer Prev, 2019; 20(4), p.1199. Doi: 10.31557/apjcp.2019.20.4.1199.
12. Abdelhameed, R.F., Habib, E.S., Eltahawy, N.A., Hassanean, H.A., Ibrahim, A.K., Mohammed, A.F., Fayez, S., Hayallah, A.M., Yamada, K., Behery, F.A. and Al-Sanea, M.M. New cytotoxic natural products from the red sea sponge *Stylissa carteri*. Mar. Drugs, 2020; 18(5), p.241. Doi: 10.3390/md18050241.
13. Hardani IN, Damara FA, Nugrahani AD, Bashari MH. Ethanol extract of *Stylissa carteri* induces cell death in parental and paclitaxel-resistant cervical cancer cells. Int. j. integr. health sci., 2018; 6(2):91-96. Doi: 10.15850/ijihs.v6n2.1378.
14. Jannah JN, Fianza PI, Putri T, Bashari MH. The ethyl acetate fraction of sponge *Stylissa carteri* decreases viability in HER2+ trastuzumab-resistant breast cancer cells. J Kedokt Kesehat Indones. 2019; 10(3):239–45. Doi: 10.20885/jkki.vol10.iss3.art6.
15. Bashari MH, Fadhil M, Aulia Y, Sari AK, Putri T, Qomarilla N, Atmaja, H., Sudji, I.R., Ariyanto, E.F., Indrati, A.R. and Rohmawaty, E. The Ethyl Acetate Fraction of Marine Sponge *Stylissa carteri* Induces Breast Cancer Cell Death via Upregulation of Mcl-1S: an In vitro Study. Asian Pac. J. Cancer Prev. 2022; 23(5):1653–1660. Doi: 10.31557/apjcp.2022.23.5.1653.
16. Pallela R, Ehrlich H. Marine sponges: Chemicobiological and biomedical applications. Marine Sponges: Chemicobiological and Biomedical Applications. 2016; 1–381. Doi: 10.1007/978-81-322-2794-2796.
17. Calcabrini C, Catanzaro E, Bishayee A, Turrini E, Fimognari C. Marine sponge natural products with anticancer potential: An updated review. Mar Drugs., 2017; 15(10), 310. Doi: 10.3390/md15100310.
18. Gomes NGM, Dasari R, Chandra S, Kiss R, Kornienko A. Marine invertebrate metabolites with anticancer activities: Solutions to the "supply problem." Mar Drugs., 2016; 14(5); 98. Doi: 10.3390/md14050098.

19. Ebada SS, Lin WH, Proksch P. Bioactive sesterterpenes and triterpenes from marine sponges: Occurrence and pharmacological significance. Mar Drugs. 2010; 8(2):313–346. Doi: 10.3390/md8020313.
20. Calado R, Mamede R, Cruz S, Leal MC. Updated Trends on the Biodiscovery of New Marine Natural Products from Invertebrates. Mar Drugs. 2022; 20(6); 389. Doi: 10.3390/md20060389.
21. Lipinski CA. Lead- and drug-like compounds: The rule-of-five revolution. Drug Discov Today Technol. 2004; 1(4):337–41. Doi: 10.1016/j.ddtec.2004.11.007.
22. Ijoma IK, Okafor CE, Ajiwe VI. Computational Studies of 5-methoxypsolaren as Potential Deoxyhemoglobin S Polymerization Inhibitor. Trop. J. Nat. Prod. Res. 2024; 8(10); 8835-8841. Doi: 10.26538/Trop. J. Nat. Prod. Res./v8i10.28.
23. Yang H, Lou C, Sun L, Li J, Cai Y, Wang Z, Li W, Liu G, Tang Y. admetSAR 2.0: web-service for prediction and optimization of chemical ADMET properties. Bioinformatics. 2019; 35(6):1067-9. Doi: 10.1093/bioinformatics/bty707.
24. KNApSAcK Core System [Internet]. 2024 [cited 2023 Jun 24]. Available from: http://www.knapsackfamily.com/knapsack_core/top.php
25. RCSB PDB: Homepage [Internet]. 2024 [cited 2023 Jun 24]. Available from: https://www.rcsb.org/
26. Way2Drug - main [Internet]. 2024 [cited 2024 Mar 31]. Available from: https://www.way2drug.com/passonline/
27. Ijoma KI, Ajiwe VI. Methyl ferulate induced conformational changes on DeOxyHbS: Implication on sickle erythrocyte polymerization. Mediterr. J. Chem. 2022; 12(1):100-11. Doi: 10.13171/mjc02208061631ijoma.
28. Dallakyan S, Olson AJ. Small-molecule library screening by docking with PyRx. Biol. methods protoc. 2015; 243-50. Doi: 10.1007/978-1-4939-2269-7_19.
29. Abraham, M.J., Murtola, T., Schulz, R., Páll, S., Smith, J.C., Hess, B. and Lindahl, E. GROMACS: High performance molecular simulations through multi-level parallelism from laptops to supercomputers. SoftwareX. 2015; 1–2:19–25. Doi: 10.1016/j.softx.2015.06.001.
30. Ghahremanian S, Rashidi MM, Raeisi K, Toghraie D. Molecular dynamics simulation approach for discovering potential inhibitors against SARS-CoV-2: A structural review. J. Mol. Liq. Elsevier B.V.; 2022; 354. Doi: 10.1016/j.molliq.2022.118901.
31. Permana S, Hanum HA, Azizah MR, Ilmiyah SZ, Permana AZ, Norahmawati E, Widodo E, Fakurazi S, Kawamoto Y, Endharti AT. *In Silico* Investigations and Potential Approaches of *Tectona grandis* via Targeting MMP-9 for Triple Negative Breast Cancer. Trop. J. Nat. Prod. Res. 2024; 8(8); 8047-8053. Doi: 10.26538/Trop. J. Nat. Prod. Res./v8i8.18.
32. Tuan ND, Quoc NC, Ly DN, Tuyen BT, Quang LD, Phien HH, De TQ, Men TT. Bioactive Extracts from *Padina boryana* Thivy from Phu Quoc Island, Vietnam: In vitro Antioxidant, Anticancer, Alpha-glucosidase inhibitory, Anti-inflammatory, Antimicrobial, and Hepatoprotective Activities. Trop. J. Nat. Prod. Res. 2024; 8(12); 9555 – 9559, Doi: 10.26538/Trop. J. Nat. Prod. Res./v8i12.29.
33. Boroujeni, M.B., Dastjerdeh, M.S., Shokrgozar, M., Rahimi, H. and Omidinia, E. Computational driven molecular dynamics simulation of keratinocyte growth factor behavior at different pH conditions. Inform. Med. Unlocked. 2021; 23, p.100514. Doi: 10.1016/j.imu.2021.100514.
34. Patel K, Laville R, Martin MT, Tilvi S, Moriou C, Gallard JF, Ermolenko L, Debitus C, Al-Mourabit A. Unprecedented Stylissazoles A–C from *Stylissa carteri*: Another Dimension for Marine Pyrrole-2-aminoimidazole Metabolite Diversity. Angew. Chem. Int. Ed. 2010; 49(28):4775-9. Doi: 10.1002/anie.201000444.
35. Wei Y, Li S, Li Z, Wan Z, Lin J. Interpretable-ADMET: a web service for ADMET prediction and optimization based on deep neural representation. Bioinform. 2022; 38(10):2863-71. Doi: 10.1002/anie.201000444.
36. Burotto M, Chiou VL, Lee JM, Kohn EC. The MAPK pathway across different malignancies: A new perspective. Cancer. John Wiley and Sons Inc.; 2014; 120. Doi: 10.1002/cncr.28864.
37. Yuan J, Dong X, Yap J, Hu J. The MAPK and AMPK signalings: Interplay and implication in targeted cancer therapy. J. Hematol. Oncol. BioMed Central Ltd; 2020. 13; 19-1. Doi: 10.1186/s13045-020-00949-4.
38. Sibuh BZ, Khanna S, Taneja P, Sarkar P, Taneja NK. Molecular docking, synthesis and anticancer activity of thiosemicarbazone derivatives against MCF-7 human breast cancer cell line. Life Sci. 2021; 273. Doi: 10.1016/j.lfs.2021.119305.
39. Moharana M, Pattanayak SK, Khan F. Molecular recognition of bio-active triterpenoids from *Swertia chirayita* towards hepatitis Delta antigen: a mechanism through docking, dynamics simulation, Gibbs free energy landscape. J Biomol Struct Dyn. 2023; 41(24):14651–64. Doi: 10.1080/07391102.2023.2184173.
40. Sharma VR, Panwar A, Sharma AK. Molecular Dynamic Simulation Study on Chromones and Flavonoids for the In Silico Designing of a Potential Ligand Inhibiting mTOR Pathway in Breast Cancer. Curr. Pharmacol. Rep. Springer Science and Business Media Deutschland GmbH; 2020; 6. 373-379, Doi: 10.1007/s40495-020-00246-1.
41. D Durrant J, McCammon AJ. Molecular Dynamics Simulations and Drug Discovery. BMC Biol. 2011; 9(71):1–9. Doi: 10.1186/1741-7007-9-71.
42. Fehske H, Schneider R, Weisse A, editors. Computational many-particle physics. Springer; 2007; 774. Doi: 10.1007/978-3-540-74686-7.
43. Gurung AB, Ali MA, Lee J, Farah MA, Al-Anazi KM. Molecular docking and dynamics simulation study of bioactive compounds from *Ficus carica* L. With important anticancer drug targets. PLoS One. 2021; 16. https://Doi: 10.1371/journal.pone.0254035.
44. Rácz A, Mihalovits LM, Bajusz D, Héberger K, Miranda-Quintana RA. Molecular Dynamics Simulations and Diversity Selection by Extended Continuous Similarity Indices. J Chem Inf Model. 2022 Jul; 62(14):3415–25. Doi: 10.1021/acs.jcim.2c00433.
45. Ghorab MM, Abdel-Kader MS, Alqahtani AS, Soliman AM. Synthesis of some quinazolinones inspired from the natural alkaloid L-norephedrine as EGFR inhibitors and radiosensitizers. J. Enzyme Inhib. Med. Chem. 2021; 36(1):218–37. Doi: 10.1080/14756366.2020.1854243.